Pressure-induced superconductivity and robust T_c against external pressure in (Ge,Sn,Pb)Te

*Ryo Matsumoto[1], Kazuki Yamane[1,2], Yoshikazu Mizuguchi[3], Rikuya Ishikawa[3], Kyohei Takae[4], Rei Kurita[3], Hidetomo Usui[5], Masahiro Ohkuma[1], Kensei Terashima[1], Yoshihiko Takano[1,2]

[1]*Research Center for Materials Nanoarchitectonics (MANA), National Institute for Materials Science, 1-2-1 Sengen, Tsukuba, Ibaraki 305-0047, Japan*

[2]*Graduate School of Pure and Applied Sciences, University of Tsukuba, 1-1-1 Tennodai, Tsukuba, Ibaraki 305-8577, Japan*

[3]*Department of Physics, Tokyo Metropolitan University, 1-1 Minami-Osawa, Hachioji, Tokyo 192-0397, Japan*

[4]*Department of Fundamental Engineering, Institute of Industrial Science, University of Tokyo, 4-6-1 Meguro-ku, Tokyo, 153-8505, Japan*

[5] *Department of Applied Physics, Shimane University, 1060 Nishikawatsu-cho, Matsue, Shimane, 690-8504, Japan*

Corresponding author; Email: MATSUMOTO.Ryo@nims.go.jp

Abstract

The robustness of superconducting transition temperature (T_c) against external pressure in medium entropy alloy (MEA) and high entropy alloy (HEA) -type compounds has attracted significant interest with regards to the realization of stable superconducting applications. In this study, we have synthesized $Ge_{1/3}Sn_{1/3}Pb_{1/3}Te$ belonging to MEA-type *M*Te, where the *M* site comprises only isovalent group-14 elements, to depict a critical factor for the robustness of T_c. High-pressure electrical transport measurements and structural analysis reveal that the high-pressure phase of CsCl-type cubic structure exhibits the robustness of T_c against external pressure. Molecular dynamics simulation and density functional theory calculation suggest that the glassy atomic vibration characteristic mainly contributes to the appearance of the robustness. This insight accelerates the further development of unique properties within HEA superconductors and their applications.

1. INTRODUCTION

High-entropy alloys (HEAs), composed of at least five elements with 5–35 at% in the composition [1-3], have attracted significant research attention because of their distinct mechanical properties, including ultrahigh fracture toughness [4-5], remarkable resistance to degradation [6], and so on [7-9]. These attributes make HEAs promising candidates for innovative applications. The tunability of charge, spin, and composition degrees of freedom within HEAs enables the design of functionality not only in mechanical performance but also in physical properties, such as achieving low thermal conductivity in thermoelectric materials [10], improved ionic conductivity [11], and enhancement of superconducting properties [12]. The advancement of HEAs paves the path for the creation of high-functionality materials.

In 2014, Ta-Nb-Zr-Hf-Ti HEA was initially discovered to exhibit superconductivity with a transition temperature (T_c) of 7.3 K [13]. One of the noteworthy characteristics of HEA superconductors is the robustness of T_c against an applying external pressure. While the T_c of simple substance Nb demonstrates a decreasing trend under external pressure, the HEA $(TaNb)_{0.67}(HfZrTi)_{0.33}$ maintains an almost constant T_c up to 190 GPa [14]. This robustness in superconductivity is believed to be associated with a reduction in Gibbs's free energy due to the elevated configuration-entropy of mixing (ΔS_{mix}), defined as $-R\sum_i c_i \ln c_i$, where R is the gas constant and c_i is the atomic ratio of the element (i). Nevertheless, the mechanism of the robustness of T_c in HEA superconductors remains an unresolved matter. The investigation of the mechanism is significant importance for the design of stable superconducting applications under compressive stress.

Recently, the concept of HEA superconductor has been successfully expanded to include "HEA-type compounds" [15]. This extension has led to the development of various HEA-type compound superconductors, such as NaCl-type metal chalcogenides *MCh* (*M* = Ag, In, Ge, Sn, Sb, Bi, Pb; *Ch* = S, Se, Te) [16-19], layered systems of $REO_{0.5}F_{0.5}BiS_2$ [20,21], high-T_c cuprates $REBa_2Cu_3O_{7-d}$ (*RE*: rare-earth elements) [22-24], and van der Waals material $(Co, Au)_{0.2}(Rh, Ir, Pd, Pt)_{0.8}Te_2$ [25]. Among them, medium entropy alloy (MEA) -type compound of $Ag_{1/3}Pb_{1/3}Bi_{1/3}Te$ ($\Delta S_{mix} = 1.1R$) and HEA-type compound of $Ag_{0.2}In_{0.2}Sn_{0.2}Pb_{0.2}Bi_{0.2}Te$ ($\Delta S_{mix} = 1.6R$) exhibit the robustness in superconductivity under external pressure in their high-pressure phase with a CsCl-type cubic structure [26]. Here, the MEA is defined as the alloy with ΔS_{mix} between 1.0*R* and 1.5*R* [3]. In contrast, the mother material PbTe ($\Delta S_{mix} = 0$) and low entropy $Sn_{0.5}Pb_{0.5}Te$ ($\Delta S_{mix} = 0.69R$) show a decrease in T_c under compression due to a reduction in the electronic density of state (DOS) at Fermi energy (E_F). High-pressure X-ray absorption spectroscopy conducted on PbTe and $Ag_{0.2}In_{0.2}Sn_{0.2}Pb_{0.2}Bi_{0.2}Te$ reveals that the DOS at E_F for *M*Te are insensitive as ΔS_{mix} increases [26]. Consequently, the mechanism behind the robust superconductivity under pressure in MEA- and HEA-type *M*Te is not solely comprehensible by considering alterations in the electronic states. Recent molecular dynamics (MD) simulations and band calculations for HEA-type *M*Te illuminate a potential mechanism for the

robustness, involving unique electron-phonon coupling in conjunction with glassy atomic vibrations and blurry electronic band dispersions [27].

However, it remains uncertain whether the glassy phonon state or the blurry electronic structure is the critical factor for this robustness. This is because of the fact that in the previous studies, the constituent elements for *M* in *M*Te have been from various groups in the periodic table, for instance, Ag, Pb, and Bi in $Ag_{1/3}Pb_{1/3}Bi_{1/3}Te$ ($\Delta S_{mix} = 1.1R$). Considering their valence states, *M*Te are basically composed of M^{2+} and Te^{2-} ions such as PbTe, while typical valence states of *M* site in $Ag_{1/3}Pb_{1/3}Bi_{1/3}Te$ are Ag^{+}, Pb^{2+} and Bi^{3+}. In such a case, the substitution of Pb^{2+} with Ag^{+} and Bi^{3+} would substantially influences both electronic and phonon states, and it is difficult to distinguish the possible main origin of the observed robustness.

In this study, we synthesize $Ge_{1/3}Sn_{1/3}Pb_{1/3}Te$ ($\Delta S_{mix} = 1.1R$), where all the elements in the *M* site belong to the same group with isovalent 2^{+}. Here, we observe the occurrence of pressure-induced superconductivity at high pressures. Remarkably, $Ge_{1/3}Sn_{1/3}Pb_{1/3}Te$ exhibits a similar robustness in T_c against pressure as the case of $Ag_{1/3}Pb_{1/3}Bi_{1/3}Te$ and $Ag_{0.2}In_{0.2}Sn_{0.2}Pb_{0.2}Bi_{0.2}Te$. Through MD simulation and first-principles calculations, $Ge_{1/3}Sn_{1/3}Pb_{1/3}Te$ exhibits broadened vibration spectrum without the presence of blurry electronic band dispersion. Our results imply that the origin of robustness in MEA- and HEA-type *M*Te is attributed to the presence of glassy phonon states in a crystal structure with enhanced ΔS_{mix}.

2. Materials and methods

Polycrystalline samples of $Ge_{1/3}Sn_{1/3}Pb_{1/3}Te$ ($\Delta S_{mix} = 1.1R$) were prepared employing a high-pressure annealing method. Starting materials of Ge powder, Sn grains, Pb grains, and Te chips were put into an evacuated quartz tube in the stoichiometric compositions of $Ge_{1/3}Sn_{1/3}Pb_{1/3}Te$. The sealed ampoule was heated at 800°C for 15 hours, followed by furnace cooling. The obtained precursors were ground into powders and pelletized into 5 mm diameter, and loaded into a hexagonal BN cell for the high-pressure annealing in a cubic-anvil-type 180-ton press to obtain NaCl-type structure. The annealing conditions of pressure, temperature, and period are 3 GPa, 500°C, and 30 min, respectively. Powder X-ray diffraction (XRD) at ambient pressure was performed on a Miniflex600 (RIGAKU) diffractometer equipped with a CuKα radiation (λ = 1.5418 Å) by the θ-2θ method. Rietveld refinement was conducted for obtained XRD pattern using RIETAN-FP software [28] to estimate the lattice constant. The crystal structure image was drawn using VESTA software [29].

The crystal structure in the obtained sample under high pressure was investigated through XRD measurements in a diamond anvil cell (DAC). These measurements were carried out utilizing synchrotron radiation at the AR-NE1A beamline of the Photon Factory (PF) situated at the High Energy Accelerator Research Organization (KEK). The X-ray beam was monochromatized to an energy of 30 keV (λ = 0.4175 Å) and introduced to the sample in the DAC through a collimator with

50 μm diameter. The XRD patterns obtained were subsequently integrated into a one-dimensional profile using IPAnalyzer [30], and the lattice constants were determined using PDIndexer [30]. High-pressure electrical transport measurements were executed within the DAC, employing a diamond electrode [31-33], and were carried out in the physical property measurement system (PPMS, Quantum Design). The sample itself and cubic BN powders were used as pressure-transmitting medium for XRD analysis and electrical measurement, respectively. The pressure in DAC was estimated by ruby fluorescence method [34] using an inVia Raman Microscope (RENISHAW).

The vibrations of atoms in *M*Te were investigated for *M*Te with NaCl-type structure using MD simulations by using the Ewald summation method. Particles *i* and *j* interact via the Lennard-Jones (LJ) and Coulomb potentials.

$$m\ddot{\boldsymbol{r}}_i = \sum_{j\neq i} \boldsymbol{F}(\boldsymbol{r_{ij}}),$$

$$\boldsymbol{F}(\boldsymbol{r_{ij}}) = -\partial U_{\mathrm{LJ}}/\partial \boldsymbol{r}_{ij} + \boldsymbol{F}_q,$$

$$U_{\mathrm{LJ}} = 4\varepsilon\left[\left(\frac{\sigma_{ij}}{r_{ij}}\right)^{12} - \left(\frac{\sigma_{ij}}{r_{ij}}\right)^{6}\right],$$

$$F_q = kq_iq_j\boldsymbol{r}_{ij}/r_{ij}^3,$$

where $\boldsymbol{r}_{ij}$ is the center-to-center displacement vector from particle *j* to *i*, $\boldsymbol{r}_{ij}$ is its absolute value, *m* is the mass common to all the particles, ε is the coefficient for LJ potential, and $\sigma_{ij} = (\sigma_i + \sigma_j)/2$, where σi is the size of particle *i*, *k* is the Coulomb constant, and q_i is the charge of particle *i*. The length of the particles was normalized by the ionic diameter of Te^{2-} (σ_{Te} = 4.42 Å). The particle sizes of Ag, Bi, Ge, Sn, and Pb are 0.520, 0.466, 0.330, 0.421, and 0.538, respectively. Here, the atomic mass *m* = 127.6 g/mol and interatomic interaction ε = 295 k_B J are assumed to be constant to elucidate the role of size and charge dispersity. We randomly arranged 6912 cation particles and 6912 Te^{2-} particles in a cubic structure. In one direction, the number of unit cells was 12. The same values as in Ref. [27] were used for the cutoff length and Ewald parameters. We calculate the vibrational density of state (VDOS) using the Fourier transformation of the velocity autocorrelation function. Details of the calculations were described in Ref. [27]. Here we note that NaCl-type structure is stable since this simulation contains no defects. However, we consider that VDOS in NaCl-type structure is similar to that in CsCl-type structure since both structures are cubic [27].

To evaluate the electronic band structure of CsCl-type *M*Te, density functional theory (DFT) calculations using the Korringa-Kohn-Rostoker Green's function method was performed in the AkaiKKR package [35]. A coherent potential approximation was used to deal the disordered structure [36]. For the calculation, the generalized gradient approximation parameterized by Perdew-Burke-Ernzerhof [37] was adapted, and spin-orbit coupling was included. The *k*-mesh of 13×13×13 was set, and the width of the energy contour for complex integration was set to 1.5 Ry. The reliability of DFT calculations was checked by the calculation of electronic structure in PbTe using WIEN2k [38].

3. Results and discussion

Figure 1 (a) presents a powder XRD pattern for the obtained $Ge_{1/3}Sn_{1/3}Pb_{1/3}Te$, along with the result from Rietveld refinement. The green bars correspond to the peak positions of the determined crystal structure, and the blue spectrum represents the differential curve in fitting. The analysis elucidates that the sample crystallizes with a NaCl-type cubic structure (*Fm-3m*) devoid of any impurity phase. The derived lattice parameters is a = 6.24887 Å with a reliability factor of R_{wp} = 5.753%. Notably, the value of a is close to that of PbTe under high pressure of 5.9 GPa (6.2492 Å), where PbTe undergoes an insulator-to-metal transition above 2 GPa [26]. This similarity can be attributed to the chemical compression effect arising from the substitution of Pb with Ge and Sn, both of which have smaller atomic radius.

Figure 1 (b) shows a temperature (T) dependence of resistivity (ρ) in $Ge_{1/3}Sn_{1/3}Pb_{1/3}Te$ at ambient pressure. The ρ-T curve in the low-temperature region is well-fitted with the Bloch-Gruneisen equation, as described by following equation [39],

$$\rho(T)=\rho_0+A\left(\frac{T}{\theta_D}\right)^5\int_0^{\theta_D/T}\frac{x^5}{(e^x-1)(1-e^{-x})}dx$$

where ρ_0 is the residual resistance, A is a characteristic constant, θ_D is the Debye temperature. The parameters are determined as ρ_0 = 1.493(4) mΩcm, A = 1.12(2), and θ_D = 125(1) K, as shown in the inset. The well-fitted ρ-T curve indicates that $Ge_{1/3}Sn_{1/3}Pb_{1/3}Te$ exhibits metallic transport nature. The θ_D is comparable with that of pristine PbTe [40]. In fig. 1 (c), the Hall resistivity of $Ge_{1/3}Sn_{1/3}Pb_{1/3}Te$ is plotted as a function of the applied magnetic field at ambient pressure to confirm carrier concentration. The carrier concentration has been estimated from the slope of Hall resistivity versus magnetic field, using the formula $\rho_H = (1/ned)H$, where ρ_H is the Hall resistivity, n is the number of carriers, e is the elementary charge, H is the magnetic field and d is the sample thickness. The ρ_H curve displays a positive slope, indicating a p-type characteristic with a carrier concentration of 1.0×10^{21} cm^{-3}. This carrier concentration significantly exceeds the typical value found in pristine PbTe, which are on the order of 10^{16} cm^{-3} [41] with an insulating nature. The elevated carrier concentration in $Ge_{1/3}Sn_{1/3}Pb_{1/3}Te$ is consistent with the metallic ρ-T behavior and is likely a result of the chemical compression effect.

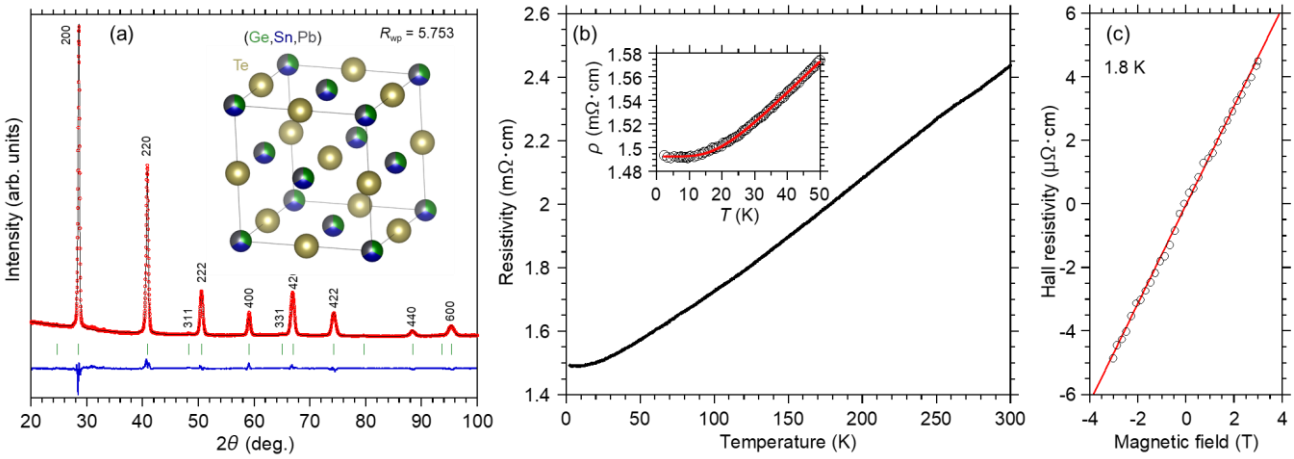

FIG. 1. (a) XRD patterns with Cu Kα radiation (λ = 1.5418 Å) of obtained $Ge_{1/3}Sn_{1/3}Pb_{1/3}Te$ with the fitting result of Rietveld refinement. The green bars and blue spectrum indicate a peak position of the determined structure and a differential curve for the fitting. (b) Temperature dependence of resistivity in $Ge_{1/3}Sn_{1/3}Pb_{1/3}Te$. The inset shows a result for the Bloch-Gruneisen fitting. (c) Hall resistivity as a function of magnetic field at 1.8 K in $Ge_{1/3}Sn_{1/3}Pb_{1/3}Te$.

Figure 2 (a) shows a temperature-dependent resistance (R) of $Ge_{1/3}Sn_{1/3}Pb_{1/3}Te$ under pressures up to 21.1 GPa. Throughout all pressure regions, a metallic R-T curve is consistently observed. The R value at 300 K continuously increases with pressure up to 8.2 GPa, after which it tends to a decreasing trend with further compression, as indicated in the inset. Notably, the R-T curve exhibits a sharp drop at 20.1 GPa and reaches zero at 1.8 K at 21.1 GPa. This drastic change in R-T curve indicates the emergence of pressure-induced superconductivity in $Ge_{1/3}Sn_{1/3}Pb_{1/3}Te$. As the pressure increases, the R value at 300 K decreases until 30 GPa and then shows a saturating trend, as presented in fig. 2 (b). The T_c demonstrates a monotonous increase as a function of pressure, reaching a plateau at 30.1 GPa, where it remains nearly constant at 5.5 K. This behavior is quite similar to other HEA-type MTe compounds [26,27].

In fig. 2 (c), XRD patterns of $Ge_{1/3}Sn_{1/3}Pb_{1/3}Te$ at various pressures up to 37 GPa are displayed. At 1.0 GPa, the observed pattern is indexed as a NaCl-type cubic structure, identical to the ambient structure. The peaks with minor intensity gradually appear above 5 GPa, leading to a complete transformation of the NaCl-type structure into the GeS-type structure at 9.0 GPa. Above 31.0 GPa, the CsCl-type cubic structure gradually becomes predominant. The phase diagram, depicting the pressure-dependent volume for each structure, is illustrated in fig. 2 (d). This pathway of structural phase transition is similar to that of other HEA-type MTe [26,27], including pristine PbTe [42]. Although the stabilized region of the intermediate GeS-type structure is more extended in $Ge_{1/3}Sn_{1/3}Pb_{1/3}Te$ compared to other MTe compounds, the underlying reason remains uncertain at present.

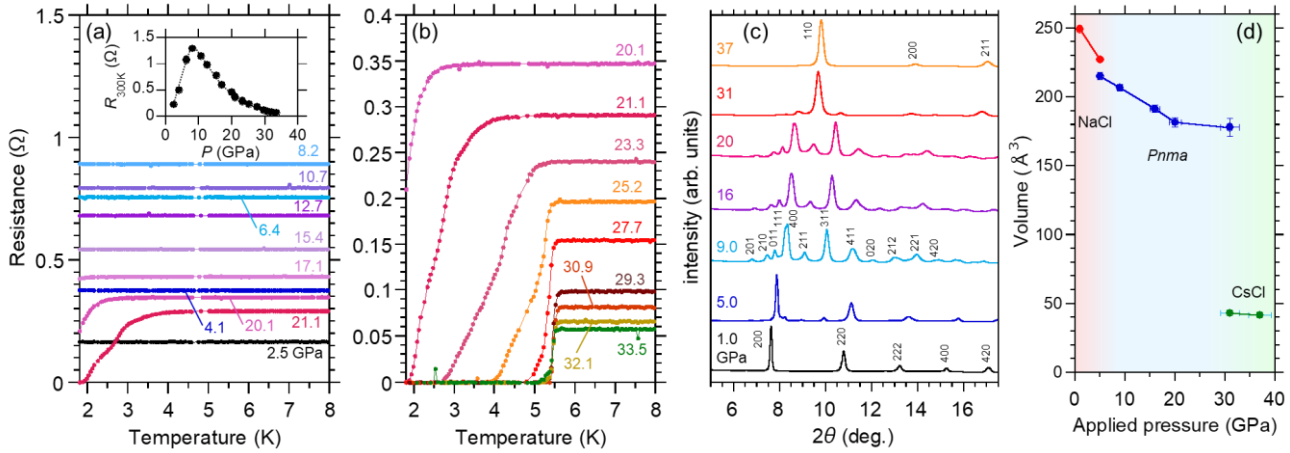

FIG. 2. Results of high-pressure experiments in $Ge_{1/3}Sn_{1/3}Pb_{1/3}Te$. (a) Temperature dependence of resistance under various pressures from 4.1 to 21.1 GPa and (b) 20.1 to 33.5 GPa. The inset in (a) shows the pressure dependence of resistance at 300 K. (c) XRD patterns under various pressures. (d) Pressure dependence of volume in each structure.

Figure 3 presents a comparison of the pressure-dependent T_c in PbTe (ΔS_{mix} = 0) [26], $Ag_{1/3}Pb_{1/3}Bi_{1/3}Te$ (ΔS_{mix} = 1.1R) [26], and $Ge_{1/3}Sn_{1/3}Pb_{1/3}Te$ (ΔS_{mix} = 1.1R). Pristine PbTe shows a drastic decline in T_c above 15 GPa, with a rate of dT_c/dP = −0.24 K/GPa, due to a reduction of electronic DOS at E_F under pressure. In contrast, $Ag_{1/3}Pb_{1/3}Bi_{1/3}Te$ exhibits a notably suppressed decreasing rate of T_c, with dT_c/dP = −0.052 K/GPa. This suppression, namely, robust T_c against pressure is considered to be related to the glassy atomic vibrations or blurry electronic structures [27]. Interestingly, $Ge_{1/3}Sn_{1/3}Pb_{1/3}Te$, where all constituent elements in the M site belong to the same group with a valence state of 2^+, also displays a robust T_c with a decreasing rate of dT_c/dP = −0.016 K/GPa. This decreasing rate is comparable to those of $Ag_{1/3}Pb_{1/3}Bi_{1/3}Te$, and $Ag_{0.2}In_{0.2}Sn_{0.2}Pb_{0.2}Bi_{0.2}Te$. It indicates that the robustness of T_c against pressure is primarily a result of the increased ΔS_{mix} and independent of the valence state of the elements within the M site.

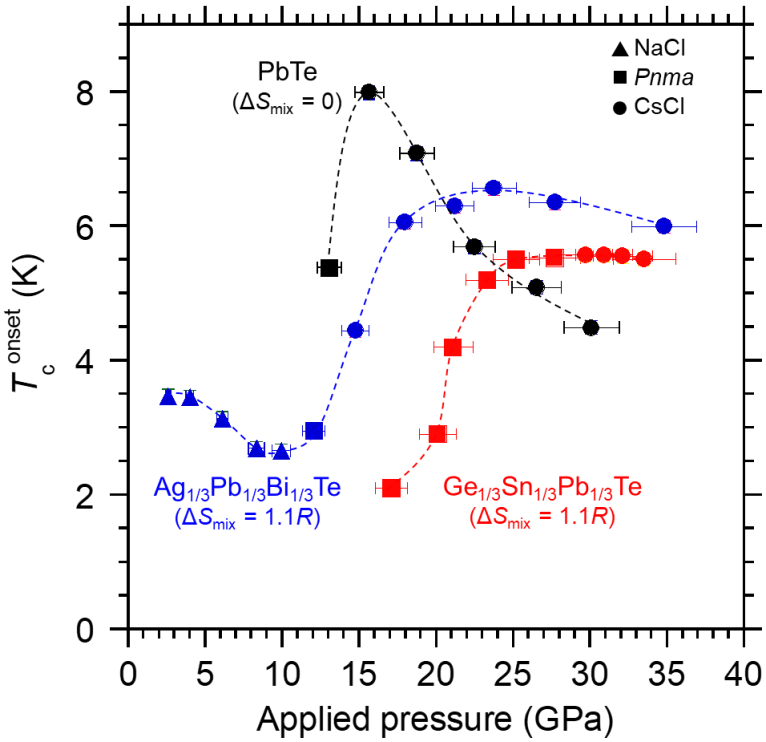

FIG. 3. Comparison of the pressure-dependent T_c in PbTe (ΔS_{mix} = 0), $Ag_{1/3}Pb_{1/3}Bi_{1/3}Te$ (ΔS_{mix} = 1.1R), and $Ge_{1/3}Sn_{1/3}Pb_{1/3}Te$ (ΔS_{mix} = 1.1R). The data of PbTe and $Ag_{1/3}Pb_{1/3}Bi_{1/3}Te$ are referred from ref [26]. The dashed lines are guides for the eye.

According to the previous reports, one possible scenario for the robustness of T_c against pressure involves the presence of glassy vibrational characteristics and/or blurry electronic structures [27]. MD simulations for atomic vibrations and DFT calculations for electronic states are conducted to delve into the mechanism behind the robust T_c. Figure 4 (a) shows the VDOS for PbTe, $Ag_{1/3}Pb_{1/3}Bi_{1/3}Te$, and $Ge_{1/3}Sn_{1/3}Pb_{1/3}Te$ calculated for the NaCl-type crystal structure. The VDOS peaks attributed to atomic vibrations exhibit a flattened profile in $Ag_{1/3}Pb_{1/3}Bi_{1/3}Te$ compared to PbTe. This broadening in the spectrum implies the presence of various vibrational modes in the material without a distinct characteristic vibration mode. The broadened VDOS is indicative of a glassy vibrational characteristic, which contributes to the robustness of T_c. The VDOS spectrum for $Ge_{1/3}Sn_{1/3}Pb_{1/3}Te$ shares a similar flat feature with $Ag_{1/3}Pb_{1/3}Bi_{1/3}Te$. The emergence of the glassy vibrational characteristic is attributed to an enhancement in ΔS_{mix}, regardless of the valence states in the M site. Figure 4 (b) presents an electronic band structure for $Ge_{1/3}Sn_{1/3}Pb_{1/3}Te$ in CsCl-type crystal structure with a=3.5Å. The band structure exhibits slight blurriness, indicating the presence of localized splitting of electronic states. In contrast, the degree of blurriness is more pronounced in $Ag_{1/3}Pb_{1/3}Bi_{1/3}Te$ [27]. The shape of the band structure in $Ge_{1/3}Sn_{1/3}Pb_{1/3}Te$ is close to that of PbTe rather than $Ag_{1/3}Pb_{1/3}Bi_{1/3}Te$. The results of MD simulation and DFT calculation collectively suggest that the primary contributor to the emergence of robust T_c against external pressure in MEA- and HEA-type MTe is the presence of broadened vibrational characteristic due to the enhancement of ΔS_{mix}.

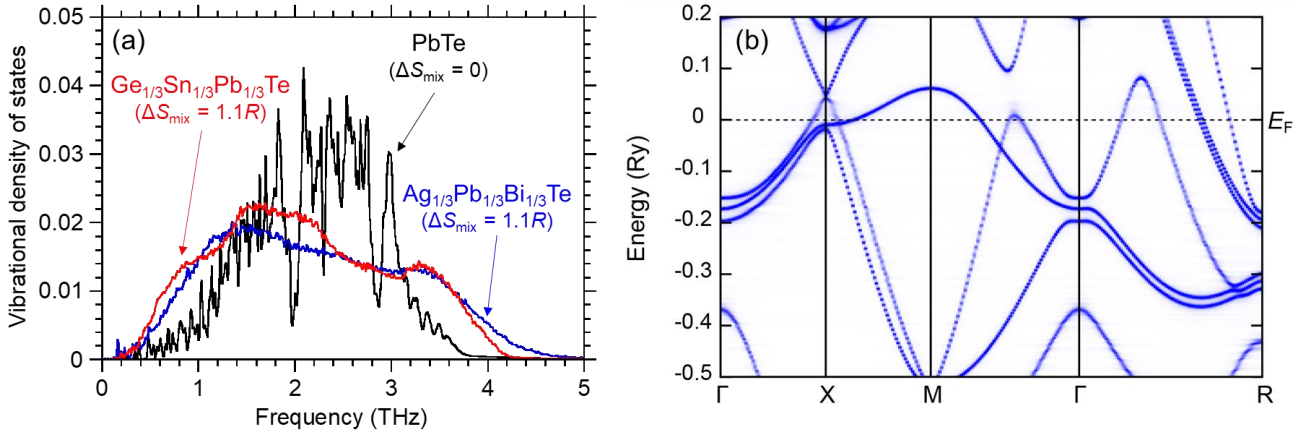

FIG. 4. (a) Simulated VDOS spectra for PbTe, $Ag_{1/3}Pb_{1/3}Bi_{1/3}Te$, and $Ge_{1/3}Sn_{1/3}Pb_{1/3}Te$. (b) Electronic band structures for $Ge_{1/3}Sn_{1/3}Pb_{1/3}Te$ at a=3.5Å.

IV. CONCLUSIONS

In this study, we synthesize $Ge_{1/3}Sn_{1/3}Pb_{1/3}Te$ belonging to MEA-type MTe family with $\Delta S_{mix} = 1.1R$, and subsequently observe the emergence of pressure-induced superconductivity. The high-pressure phase of the CsCl-type cubic structure shows almost constant pressure-dependent T_c, namely, the appearance of the robustness of T_c against external pressure. Based on the MD simulations and DFT calculations, it was turned out that the robust T_c persists in $Ge_{1/3}Sn_{1/3}Pb_{1/3}Te$ where the broadened VDOS exists without the blurry electronic band dispersions. Our current study implies that the unique phonon state due to the enhancement of ΔS_{mix} plays a crucial role to induce the robust T_c in MEA- and HEA-type MTe. This insight holds significant importance for advancing our understanding of the mechanisms behind the robustness of T_c and in developing stable superconducting applications under compressive stress.

ACKNOWLEDGMENTS

This work was partly supported by JSPS KAKENHI Grant Number 23K13549. The fabrication process of diamond electrodes was partially supported by the NIMS Nanofabrication Platform in the Nanotechnology Platform Project sponsored by the Ministry of Education, Culture, Sports, Science and Technology (MEXT), Japan. The synchrotron X-ray experiments were performed at AR-NE1A (KEK-PF) under the approval of Proposal No. 2022G049 with support from Dr. Y. Shibazaki (KEK).

References

[1] J. W. Yeh, S. K. Chen, S. J. Lin, J. Y. Gan, T. S. Chin, T. T. Shun, C. H. Tsau, and S. Y. Chang, Nanostructured High-Entropy Alloys with Multiple Principal Elements, Adv. Energy Mater. 6 (2004) 299.

[2] B. Cantor, I. T. H. Chang, P. Knight, A. J. B. Vincent, Microstructural Development in

Equiatomic Multicomponent Alloys. Mater. Sci. Eng. 375−377 (2004) 213−218.

[3] S. Akrami, P. Edalati, M. Fuji, K. Edalati, High-entropy ceramics: Review of principles, production and applications, Mater. Sci. Eng. R 146 (2021) 100644.

[4] B. Gludovatz, A. Hohenwarter, K. V. S. Thurston, H. Bei, Z. Wu, E. P. George, R. O. Ritchie, Exceptional damage-tolerance of a medium-entropy alloy CrCoNi at cryogenic temperatures, Nat. Commun. 7 (2016) 10602.

[5] X. J. Fan, R. T. Qu, Z. F. Zhang, Remarkably high fracture toughness of HfNbTaTiZr refractory high-entropy alloy, J. Mater. Sci. Technol. 123 (2022) 70-77.

[6] J. Shittu, M. Pole, I. Cockerill, M. Sadeghilaridjani, L. V. K. Reddy, G. Manivasagam, H. Singh, H. S. Grewal, H. S. Arora, S. Mukherjee, Biocompatible High Entropy Alloys with Excellent Degradation Resistance in a Simulated Physiological Environment, ACS Appl. Bio Mater. 3 (2020) 8890–8900.

[7] K. M. Youssef, A. J. Zaddach, C. Niu, D. L. Irving, C. C. Koch, A novel low-density, high-hardness, high-entropy alloy with close-packed single-phase nanocrystalline structures. Mater. Res. Letters 3 (2016) 95–99.

[8] H. Kou, J. Lu, Y. Li, High-strength and high-ductility nanostructured and amorphous metallic materials. Adv, Mater. 26 (2014) 5518–5524.

[9] Y. Zou, H. Ma, R. Spolenak, Ultrastrong ductile and stable high-entropy alloys at small scales. Nat. Commun. 6 (2015) 7748.

[10] B. Jiang, Y. Yu, J. Cui, X. Liu, L. Xie, J. Liao, Q. Zhang, Y. Huang, S. Ning, B. Jia, B. Zhu, S. Bai, L. Chen, S. J. Pennycook, J. He, High-entropy-stabilized chalcogenides with high thermoelectric performance, Science 371 (2021) 830-834.

[11] F. Strauss, J. Lin, M. Duffiet, K. Wang, T. Zinkevich, A. L.Hansen, S. Indris, and T. Brezesinski, High-entropy polyanionic lithium superionic conductors, ACS Materials Lett. 4 (2022) 418.

[12] B. Liu, W. Yang, G. Xiao, Q. Zhu, S. Song, G. H. Cao , Z. Ren, High-entropy silicide superconductors with W_5Si_3-type structure, Phys. Rev. Mater. 7 (2023) 014805.

[13] P. Koželj, S. Vrtnik, A. Jelen, S. Jazbec, Z. Jagličić, S. Maiti, M. Feuerbacher, W. Steurer, and J. Dolinšek, Discovery of a Superconducting High-Entropy Alloy, Phys. Rev. Lett. 113 (2014) 107001.

[14] J. Guo, H. Wang, F. von Rohr, Z. Wang, S. Cai, Y. Zhou, K. Yang, A. Li, S. Jiang, Q. Wu, R. J. Cava, and L. Sun, Robust zero resistance in a superconducting high-entropy alloy at pressures up to 190 GPa, PNAS 114 (2017) 13144.

[15] Y. Mizuguchi and A. Yamashita, Superconductivity in HEA-Type Compounds, IntechOpen (2021).

[16] Y. Mizuguchi, Superconductivity in high-entropy-alloy telluride $AgInSnPbBiTe_5$, J. Phys.

Soc. Jpn. 88 (2019) 124708.

[17] Md. R. Kasem, K. Hoshi, R. Jha, M. Katsuno, A. Yamashita, Y. Goto, T. D. Matsuda, Y. Aoki, Y. Mizuguchi, Superconducting properties of high-entropy-alloy tellurides M-Te (M: Ag, In, Cd, Sn, Sb, Pb, Bi) with a NaCl-type structure, Appl. Phys. Express 13 (2020) 033001.

[18] A. Yamashita, R. Jha, Y. Goto, T. D. Matsuda, Y. Aoki, Y. Mizuguchi, An efficient way of increasing the total entropy of mixing in high-entropy-alloy compounds: a case of NaCl-type (Ag,In,Pb,Bi)$Te_{1-x}Se_x$ (x = 0.0, 0.25, 0.5) superconductors, Dalton Trans. 49 (2020) 9118.

[19] Md. R. Kasem, R. Ishii, T. Katase, O. Miura, Y. Mizuguchi, Tuning of carrier concentration and superconductivity in high-entropy-alloy-type metal telluride $(AgSnPbBi)_{(1-x)/4}In_xTe$, J. Alloys Compd. 920 (2022) 166013.

[20] R. Sogabe, Y. Goto, Y. Mizuguchi, Superconductivity in $REO_{0.5}F_{0.5}BiS_2$ with high-entropy-alloy-type blocking layers, Appl. Phys. Express 11 (2018) 053102.

[21] Y. Fujita, K. Kinami, Y. Hanada, M. Nagao, A. Miura, S. Hirai, Y. Maruyama, S. Watauchi, Y. Takano, I. Tanaka, Growth and characterization of $ROBiS_2$ high-entropy superconducting single crystals, ACS Omega 5 (2020) 16819.

[22] Y. Shukunami, A. Yamashita, Y. Goto, Y. Mizuguchi, Synthesis of RE123 high-T_c superconductors with a high-entropy-alloy-type RE site, Physica C 572 (2020) 1353623.

[23] K. Wang, Q. Hou, A. Pal, H. Wu, J. Si, J. Chen, S. Yu, Y. Chen, W. Lv, J.Y. Ge, S. Cao, J. Zhang, Z. Feng, Structural and physical properties of high-entropy $REBa_2Cu_3O_{7-\delta}$ oxide superconductors, J. Supercond. Nov. Magnetism 34 (2021) 1379.

[24] A. Yamashita, K. Hashimoto, S. Suzuki, Y. Nakanishi, Y. Miyata, T. Maeda, Y. Mizuguchi, Fabrication of high-entropy $REBa_2Cu_3O_{7-\delta}$ thin films by pulsed laser deposition, Jpn. J. Appl. Phys. 61 (2022) 050905.

[25] T. Ying, T. Yu, Y. S. Shiah, C. Li, J. Li, Y. Qi, H. Hosono, High-Entropy van der Waals Materials Formed from Mixed Metal Dichalcogenides, Halides, and Phosphorus Trisulfides, J. Am. Chem. Soc. 143 (2021) 7042−7049.

[26] M.d R. Kasem, Y. Nakahira, H. Yamaoka, R. Matsumoto, A. Yamashita, H. Ishii, N. Hiraoka, Y. Takano, Y. Goto, Y. Mizuguchi, Robustness of superconductivity to external pressure in high-entropy-alloy-type metal telluride $AgInSnPbBiTe_5$, Sci. Rep. 12 (2022) 7789.

[27] Y. Mizuguchi, H. Usui, R. Kurita, K. Takae, Md. R. Kasem, R. Matsumoto, K. Yamane, Y. Takano, Y. Nakahira, A. Yamashita, Y. Goto, A. Miura, C. Moriyoshi, Glassy atomic vibrations and blurry electronic structures created by local structural disorders in high-entropy metal telluride superconductors, Mater. Today Phys. 32 (2023) 101019.

[28] F. Izumi, K. Momma, Three-dimensional visualization in powder diffraction, Solid State Phenom. 130 (2007) 15.

[29] K. Momma, F. Izumi, VESTA: a three-dimensional visualization system for electronic and

structural analysis, J. Appl. Crystallogr. 41 (2008) 653.

[30] Y. Seto, D. Hamane, T. Nagai, K. Fujino, Fate of carbonates within oceanic plates subducted to the lower mantle, and a possible mechanism of diamond formation, Phys. Chem. Miner. 35 (2008) 223-229.

[31] R. Matsumoto, Y. Sasama, M. Fujioka, T. Irifune, M. Tanaka, T. Yamaguchi, H. Takeya, and Y. Takano, Note: Novel diamond anvil cell for electrical measurements using boron-doped metallic diamond electrodes, Rev. Sci. Instrum. 87 (2016) 076103.

[32] R. Matsumoto, T. Irifune, M. Tanaka, H. Takeya, and Y. Takano, Diamond anvil cell using metallic diamond electrodes, Jpn. J. Appl. Phys. 56 (2017) 05FC01.

[33] R. Matsumoto, H. Hara, H. Tanaka, K. Nakamura, N. Kataoka, S. Yamamoto, T. Irifune, A. Yamashita, S. Adachi, H. Takeya, Y. Takano, Pressure-induced superconductivity in sulfur-doped SnSe single crystal using boron-doped diamond electrode-prefabricated diamond anvil cell, J. Phys. Soc. Jpn. 87 (2018) 124706.

[34] H. K. Mao, P. M. Bell, J. W. Shaner, D. J. Steinberg, Specific volume measurements of Cu, Mo, Pd, and Ag and calibration of the ruby R1 fluorescence pressure gauge from 0.06 to 1 Mbar, J. Appl. Phys. 49 (1978) 3276-3283.

[35] H. Akai, Electronic structure Ni–Pd alloys calculated by the self-consistent KKR-CPA method, J. Phys. Soc. Jpn. 51 (1982) 468.

[36] H. Ebert, D. Ködderitzsch, J Minár, Calculating condensed matter properties using the KKR-Green's function method—recent developments and applications, Rep. Prog. Phys. 74 (2011) 096501.

[37] J. P. Perdew, K. Burke, M. Ernzerhof, Generalized gradient approximation made simple, Phys. Rev. Lett. 77 (1996) 3865.

[38] P. Blaha, K. Schwarz, F. Tran, R. Laskowski, G. K. H. Madsen, L. D. Marks, WIEN2k, An APW+lo program for calculating the properties of solids, J. Chem. Phys. 152 (2020) 074101.

[39] J. M. Ziman, Electrons and Phonons: The Theory of Transport Phenomena in Solids, Oxford Classic Texts in the Physical Sciences (Clarendon, Oxford, 2001).

[40] R. Minikayev, F. Safari, A. Katrusiak, W. Szuszkiewicz, A. Szczerbakow, A. Bell, E. Dynowska, W. Paszkowicz, Thermostructural and Elastic Properties of PbTe and $Pb_{0.884}Cd_{0.116}Te$: A Combined Low-Temperature and High-Pressure X-ray Diffraction Study of Cd-Substitution Effects, Crystals 11 (2021) 1063.

[41] M. P. Dariel, Z. Dashevsky, A. Jarashnely, S. Shusterman, A. Horowitz, Carrier concentration gradient generated in p-type PbTe crystals by unidirectional solidification, J. Cryst. Growth 234 (2002) 164-170.

[42] Y. Fujii, K. Kitamura, A. Onodera, Y. Yamada, A new high-pressure phase of PbTe above 16 GPa, Solid State Commun. 49, 135-139 (1984).